# Assessment of spherical blast wave models

Caio Barbosa Amorim[1], Rene Francisco Boschi Gonçalves[1], Koshun Iha[1]
[1]Instituto Tecnológico de Aeronáutica (ITA), São José dos Campos/SP – Brasil

***Abstract* – Detonations—whether accidental or intentional—are part of modern society, and the resulting blast wave is among their most destructive consequences. High-speed footage offers a safe and practical means of acquiring data from such events, enabling the indirect estimation of peak overpressure—an essential parameter for damage assessment. This study presents a case involving the detonation of four spherical charges of plastic-bonded explosive based on Octogen. Empirical data were collected using high-speed video and pressure gauges; while footage was used for model fitting, both data sources were employed to assess model performance. Among the seven evaluated models, only the one proposed by Amorim, Silva, and Gonçalves showed strong agreement with experimental data, accurately estimating both the peak overpressure and the detonation onset time, and yielding a well-behaved residual distribution.**

***Keywords* – footage, blast wave, peak overpressure.**

## I. INTRODUCTION

Materials capable of undergoing detonation are widely used in both civilian and military applications, prompting extensive research aimed at understanding and modeling the phenomenon. Among its effects, the resulting blast wave poses a particular challenge, as it can propagate over large distances and cause severe damage.

In light of this, the present study assesses the performance of existing models in the literature in accurately capturing blast wave dynamics. This assessment is based on a case study involving the detonation of four center-initiated spherical charges of plastic-bonded explosive (PBX) based on Octogen (HMX), with data acquired via high-speed footage and pressure gauges.

As a spherical blast wave propagates through air, it expands over time and reaches an approximately spherical surface of a certain radius (r) at the corresponding time of arrival ($t_a$). At this moment, the atmospheric pressure abruptly increases by an amount known as peak overpressure ($P_{so}$), marking the beginning of the so-called positive phase. This phase lasts for a duration ($t_d$) until the pressure returns to the ambient level ($P_0$). The integral of the overpressure during this interval is referred to as the positive phase impulse ($I_+$). The typical pressure-time profile resulting from such an event is illustrated in Fig. 1.

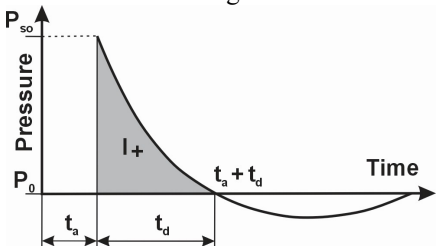


Fig. 1. Pressure–time profile generated by the passage of a blast wave through air.

C. B. Amorim, caiocba@fab.mil.br; R. F. B. Gonçalves, renefbg@ita.br; K. Iha, koshuniha@gmail.com; W. M. de Melo, wandeclaytwmm@fab.mil.br.

Blast wave damage assessment typically relies on iso-damage curves derived from Pressure-Impulse diagrams, which use only $P_{so}$ and $I_+$ as input parameters [1]. Therefore, accurate estimation of these two parameters is of critical importance; however, damage analyses sometimes report only $P_{so}$ [2]. Specifically, $P_{so}$ can be calculated from r versus $t_a$ data using the Rankine-Hugoniot relations [3], as shown in Eq. (1), where $a_0$ represents the ambient sound speed. This implies that $P_{so}$ can be indirectly determined from high-speed footage, which is preferable to direct measurements because it allows data acquisition from a safe distance.

$$P_{so} = 7P_0/6\{[(dr/dt_a)/a_0]^2-1\} \quad (1)$$

However, this method presents the challenge of accurately calculating the derivative of r with respect to $t_a$. A practical alternative to address this issue is the use of parametric fitted models for the r versus $t_a$ data, which can be easily differentiated to estimate $P_{so}$ with reduced uncertainty. A comprehensive literature review was conducted to identify existing models developed for this purpose, resulting in the selection of seven different models [4]-[10].

The models were fitted to radius-time data extracted from high-speed footage and assessed based on residual analysis, as well as the accuracy of $P_{so}$ and detonation time ($t_0$) estimation. The reference $P_{so}$ values were obtained from direct measurements using five pressure gauges at three different distances.

The results showed that only three models [4],[8],[10] produced reliable $P_{so}$ estimates at the measurement locations, although two of them exhibited high uncertainty for at least one of the estimations [4],[8]. These three models also displayed satisfactory residual distributions. However, only one model [10] was able to accurately estimating $t_0$.

## II. MATERIALS AND METHODS

The four tests, designated T1 through T4, were conducted according to the experimental setup described in [11]. The most relevant aspects are summarized bellow.

Each of the four charges consisted of a PBX formulation containing 80% HMX. The charges were spherically shaped, center-initiated, and has masses ranging from 241.5 g to 247.9 g. The setup, illustrated in Fig. 2, included a wooden structure for image calibration, five pressure gauges (labeled S1 to S5), and a high-speed camera. The parameters shown in Fig. 2 are detailed in Table I.

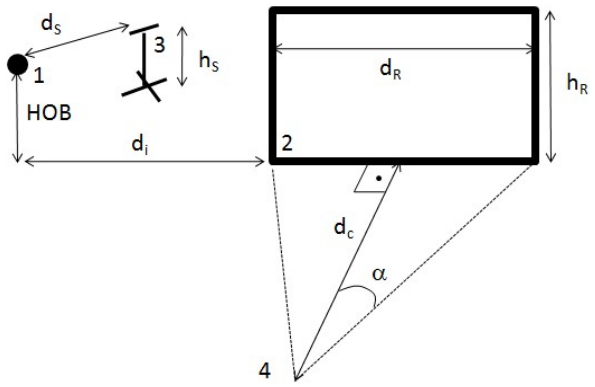


Fig. 2. Tests setup presenting the positioning of the explosive charge (1), the wood structure for image calibration (2), the pressure gauges (3) and the high-speed camera (4).

TABLE I. SETUP PARAMETERS DESCRIPTIONS AND VALUES

| *Symbol* | *Description* | *Value* |
|---|---|---|
| α (º) | Camera to structure edges horizontal angle | 2.5 |
| $d_c$ (m) | Camera to structure distance | 23 |
| $d_i$ (m) | Charge to structure horizontal distance | 1.30 (T1 to T3)<br>2.30 (T4) |
| $d_R$ (m) | Structure width | 2.00 |
| $d_S$ (m) | Charge to pressure gauges distance | 1.45 (S1)<br>1.9 (S2-S3)<br>2.4 (S4-S5) |
| HOB (m) | Height of burst | 0.8 |
| $h_S$ (m) | Pressure gauge height | 0.88 (S1)<br>1.6 (S2-S3)<br>1.7 (S4-S5) |

The high-speed camera model used for the footage was the Olympus iSpeed TR, operating at a frame rate of 5,000 fps, corresponding to a time frame (T) of 0.002 s. $P_{so}$ measurements were obtained using High Pressure Instruments (HPI) model B251 pressure gauges, positioned at distances of 1.45 m, 1.9 m, and 2.4 m from the detonation center. Calibration was enabled by the wooden structure, which featured distance markers as shown in Fig. 3. Radius measurements were obtained by averaging five samples for each time instant and computing the 95% confidence interval (CI95), which yielded a mean CI95 span of 2 cm. Parallax correction was applied using the algorithm described in [10].

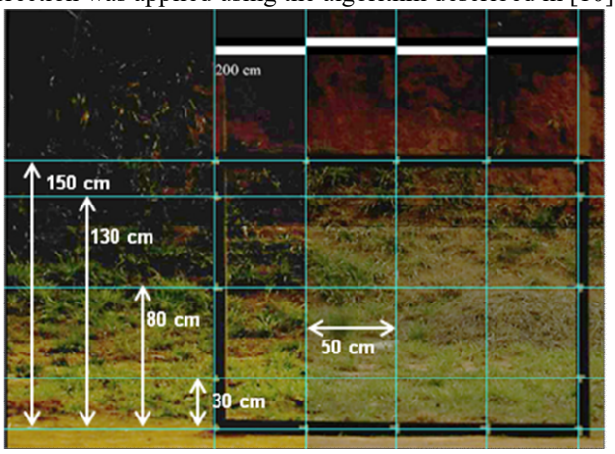


Fig. 3. Wooden structure calibration marks and respective distances.

The models identified in the literature and selected for comparison in this study are listed and described in Table II. All models were adjusted to start at the charge radius (R) when $t_a = 0$, by adding a constant term when necessary. The equation and the suitability analysis for each model are detailed in a previous study [10].

TABLE II. LITERATURE MODELS SPECIFICATION

| *Model* | *Reference* |
|---|---|
| M1 | [4] |
| M2 | [5] |
| M3 | [3] |
| M4 | [7] for $t_a$ versus r |
| M5 | [8] |
| M6 | [9] |
| M7 | [10] |

An additional parameter, $t_0$, was included in each model to evaluate their qualitative ability to estimate the detonation moment, which closely corresponds to the onset of the blast wave. The footage timeline was defined to begin at the first frame showing evidence of the detonation reaction. However, the total blast wave propagation time should have the addition of $t_0$, which is expected to lie within the interval [0, T]. In cases where the initial frame reflects only the initiator's detonation, $t_0$ may be slightly negative. Therefore, for the purposes of this study, $t_0$ was bounded between –T and T.

Each model was fitted to the footage-derived radius-time data from each test, and its $t_0$ estimation accuracy was then assessed. Initial models optimization was performed without constraints on $t_0$, in order to evaluate the model's intrinsic accuracy in estimating this parameter. If the CI95 of the resulting $t_0$ fell outside the [-T, T] range, the model was re-optimized with $t_0$ fixed to the closest bound (either –T or T), to proceed with the subsequent analysis, starting with the residual assessment.

Next, the models fitted for the radius-time data for each test were used to estimate $P_{so}$ at each distance corresponding to the pressure gauge locations. The results from all four tests were then averaged for each model—except in the residual analysis, where the worst-case scenario was selected for comparison. Finally, the CI95 values estimated for $P_{so}$ at each distance were compared against to the CI95 values obtained from the experimental pressure gauge measurements across all tests.

## III. RESULTS AND DISCUSSIONS

The first analysis focused the models' ability to accurately estimate $t_0$. Fig. 4 displays the blast wave position-time graphs for the four tests. As expected, the curves are very similar; however, noticeable differences can be observed, primarily due to variations in their $t_0$ values. In this regard, Fig. 4 shows that test T4 has the highest $t_0$ value, which is similar to that of test T3. Test T2 exhibits an intermediate value between test T3 and test T1, the latter having the lowest $t_0$ value among all tests.

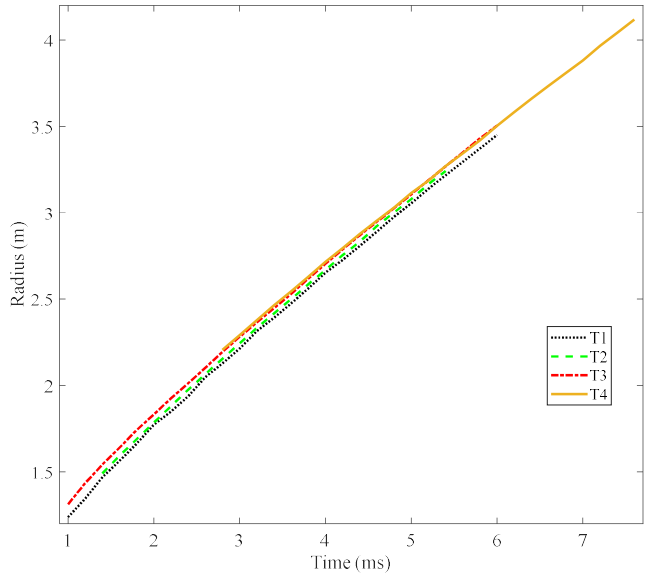


Fig. 4. Blast wave position-time graph for each test.

Table III presents the CI95 values for $t_0$ obtained from the initial optimization of each model. As shown in the table, all models—except M6 and M7—produced at least one $t_0$ estimate with its CI95 outside the defined physical boundaries. Among these two, only the results from model M7 are consistent with the $t_0$ behavior discussed in the last paragraph and illustrated in Fig. 4.

TABLE III. INITIAL OPTIMIZATION CI95 FOR EACH TEST

| $t_0/T$ | *T1* | *T2* | *T3* | *T4* |
|---|---|---|---|---|
| M1 | 1.1 ± 0.5 | 1.9 ± 0.6 | 1.8 ± 0.4 | 2 ± 1 |
| M2 | -1.2 ± 0.2 | -1.2 ± 0.3 | -0.6 ± 0.2 | -1.7 ± 0.2 |
| M3 | 0 ± 2 | 6 ± 4 | -1 ± 0.5 | 4 ± 3 |
| M4 | -1 ± 1 | -1 ± 0.7 | -4 ± 1 | -3 ± 2 |
| M5 | -1.75 ± 0.09 | -1.79 ± 0.09 | -1.2 ± 0.09 | -2.85 ± 0.04 |
| M6 | 0.1 ± 0.2 | 0.3 ± 0.2 | 0.8 ± 0.2 | 0.3 ± 0.2 |
| M7 | 0.3 ± 0.1 | 0.4 ± 0.1 | 1 ± 0.1 | 1.1 ± 0.1 |

As emphasized in the previous section, for the cases in Table III where $t_0$ falls outside the interval [-T, T], the model was re-optimized by setting $t_0$ to the nearest bound for the subsequent analysis. The models were then evaluated based on their Pearson residuals from the optimization, as presented in Fig. 5.

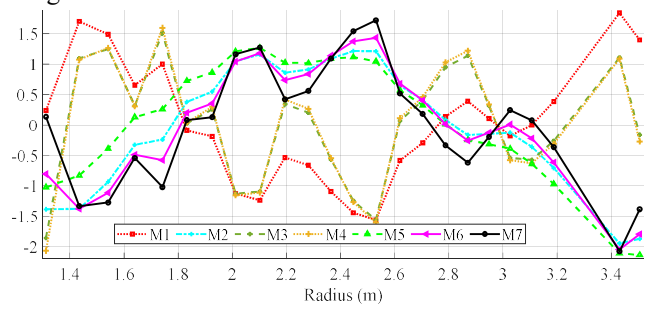


Fig. 5. Pearson residuals plot for a worst-case scenario.

Models M3 and M4 produced residual plots that more closely resembled the expected pattern, with points randomly scattered around an mean value of zero. Meanwhile, models M1 and M7 exhibited shape deviations from the expected shape near the plot boundaries. The remaining models—M2, M5, and M6—displayed non-random patterns throughout the entire plot.

The final analysis aimed to assess whether the models were capable of estimating $P_{so}$—in its scaled form $P_{so}/P_0$, where $P_0$ was approximately 0.95 bar—in agreement with the experimental results. Table IV presents the CI95 values for the pressure gauge measurements at each distance across all the tests, as well as the CI95 values corresponding to the estimates obtained from each model.

TABLE IV. PEAK OVERPRESSURE CI95 COMPARISON

| $P_{so}/P_0$ | *1.45 m* | *1.9 m* | *2.4 m* |
|---|---|---|---|
| Measured | 1.6 ± 0.1 | 0.95 ± 0.05 | 0.61 ± 0.02 |
| M1 | 1.7 ± 0.2 | 0.98 ± 0.05 | 0.62 ± 0.02 |
| M2 | 2.2 ± 0.3 | 1.1 ± 0.1 | 0.59 ± 0.07 |
| M3 | 2 ± 2 | 1.1 ± 0.4 | 0.62 ± 0.03 |
| M4 | 1.64 ± 0.09 | 0.91 ± 0.04 | 0.61 ± 0.05 |
| M5 | 2.32 ± 0.09 | 1.03 ± 0.04 | 0.51 ± 0.05 |
| M6 | 2 ± 0.2 | 1.1 ± 0.1 | 0.62 ± 0.06 |
| M7 | 1.76 ± 0.05 | 0.98 ± 0.03 | 0.61 ± 0.02 |

As shown in Table IV, only models M1 and M4 produced CI95 intervals that partially overlapped with those from the experimental measurements. However, model M1 exhibited a large relative CI95 span at 1.45 m, while model M4 showed a similar issue at 2.4 m, which may render their practical application unfeasible. In contrast, model M7's CI95 did not overlap with the measurement intervals only at 1.45 m—and even then, the discrepancy was minor. Notably, model M7 maintained a consistent and narrow CI95 span of approximately 6% across all distances, which is sufficiently tight for practical use. For instance, models M2, M5, and M6 produced estimates that fell outside the experimental CI95 range at more than one distance, while model M3 exhibited excessively high uncertainty at 1.45 m and 1.9 m.

Overall, only model M7 demonstrated satisfactory performance across all evaluation criteria. This was particularly evident in the estimation of $t_0$, where it was the only model to consistently align with the experimental data. Furthermore, model M7 performed acceptably in both the residuals analysis and the estimation of $P_{so}$, indicating strong consistency.

These findings are in agreement with a similar analysis conducted using a different empirical dataset [10], further supporting the suitability of model M7 for practical applications. Therefore, this model can be reliably used to process empirical blast wave footage and estimate $P_{so}$ at some specific locations of interest. Ultimately, it can be concluded that model M7 enables accurate and reliable damage assessment.

## IV. CONCLUSION

As materials capable of detonation are widely used across various sectors, there is a growing need to study the resulting blast wave, particularly due to its potential to cause damage over long distances. In this context, developing accurate models for estimating blast effects using footage is of great interest, as it enables safer more accessible experimental data acquisition.

The primary parameters used for blast wave damage assessment are peak overpressure and positive phase impulse, with this study focusing on the former. Parametric model fitting offers a feasible method for estimating with low uncertainty. A comprehensive literature review identified seven existing models (M1–M7), which were compared in this work.

The comparison was based on a case study involving four similar tests (T1–T4). The experimental setup included a high-speed camera operating at 5,000 fps and five pressure gauges placed at three distances: 1.45 m, 1.9 m, and 2.4 m. Each test involved the detonation of a center-initiated spherical PBX charge (~245 g, 80% HMX).

Model performance was evaluated across three criteria:

1. **Estimation of the detonation moment ($t_0$)**: Models were assessed based on their ability to estimate $t_0$ within the physically acceptable range [-T, T] and whether the results aligned qualitatively with the position–time data. If a model failed this criterion, it was re-optimized with $t_0$ fixed at the nearest boundary.
2. **Residual analysis**: This evaluated whether each model produced residuals with a random distribution centered around zero in the worst-case scenario.
3. **Estimation of $P_{so}$**: Model predictions were compared to pressure gauge measurements, using confidence intervals to assess accuracy and uncertainty.

The $t_0$ analysis showed that only models M6 and M7 estimated values within the physical boundaries for all tests. However, only model M7 provided results consistent with the observed sequence in the position-time plots, where T4 and T3 had the highest $t_0$ values and T1 the lowest.

Residual analysis indicated that M3 and M4 had the most desirable residual distributions. Models M1 and M7 deviated from the expected pattern only at the plot boundaries, while the remaining models showed non-random behavior throughout.

In terms of $P_{so}$ estimation, only models M1 and M4 produced results within the experimental confidence intervals—but with relatively high uncertainty at one of the distances, limiting their practical applicability. Model M7 failed to match the experimental interval only at the closest distance, and the discrepancy was minor. Additionally, M7 consistently maintained narrow confidence intervals (~3%), supporting its reliability.

The $P_{so}$ estimation assessment revealed that the only models able to do it accordingly, M1 and M4, did it with a relatively high uncertainty for at least one of the distances. This can render them of no practical use. Model M7, however, just did not fit the measurements interval of confidence for the closest distance, although the gap was small and the prediction uncertainty was always narrow. The other models had poor estimation issues for at least one distance.

In conclusion, model M7 demonstrated the best overall performance. It was the only model to accurately estimate $t_0$ in agreement with empirical data, showed acceptable residual behavior, and delivered precise $P_{so}$ estimations with minimal uncertainty. These findings are consistent with a previous study based on a different dataset [10], reinforcing the practical applicability of model M7 for damage assessment based on footage data from blast wave experiments.

## REFERENCES


[1] L. Chernin, M. Vilnay, I. Shufrin, D. Cotsovos, “Pressure-impulse Diagram Method—A Fundamental Review”, Proc. Inst. Civ. Eng. Eng. Comput. Mech., vol. 172, p. 55–69, 2019.

[2] F. B. Mendonça, K. Iha, G. F. M. Pinheiro, C. B. Amorim, J. A. F. F. Rocco, “Comportamento de uma laje de concreto armado submetida aos efeitos da onda de choque oriunda da detonação de explosivo plástico de uso militar”, Spectrum, vol. 22, p. 25-29, 2021.

[3] G. F. Kinney, Kenneth J. Graham,. “Explosive Shocks in Air”, 2ed., New York, NY: Springer-Verlag, 1985.

[4] J. M. Dewey, “The properties of a blast wave obtained from an analysis of the particle trajectories”, in Proc. R. Soc. *A*, vol. 324, p. 275-299, 1971.

[5] D. L. Jones, “Intermediate Strength Blast Waves”, Phys. Fluids, vol. 11, p. 1664-1667, 1968.

[6] H. S. Sadek, J. J. Gott1ieb, “Initial decay of flow properties of planar, cylindrical and spherical blast waves”, Toronto, 1983.

[7] T. Wei, M. J. Hargather, “A new blast wave scaling”, Shock Waves, vol. 31, p. 231-238, 2022.

[8] J. S. Díaz, S. E. Rigby, “Blast wave kinematics: theory, experiments, and applications”, Shock Waves, vol. 32, p. 405-415, 2022.

[9] C. N. Kingery; G Bulmash, “Airblast parameters from spherical air burst and hemispherical surface burst”, Aberdeen, 1984.

[10] C. B. Amorim, A. A. Silva, R. F. B. Gonçalves. “A constant trinitrotoluene equivalence fit for blast wave position versus time data”. Propellants, Explos., Pyrotech., vol. 50, p. 44-54, 2025.

[11] C. B. Amorim, “Estudo experimental da dinâmica e dos parâmetros de efeito de sopro da onda de Mach”, dissertação de mestrado, Instituto Tecnológico de Aeronáutica, São José dos Campos, 2016.